Claudia Dannehl, Gerald Brezesinski, and Helmuth Möhwald*

# Interactions of Two Fragments of the Human Antimicrobial Peptide LL-37 with Zwitterionic and Anionic Lipid Monolayers

DOI 10.1515/zpch-2014-0565
Received July 9, 2014; accepted November 14, 2014

**Abstract:** The interactions of two fragments of the human antimicrobial LL-37 (LL-32 and LL-20) with lipid monolayers at the soft liquid/air interface have been characterized. To model the interaction with mammalian cell membranes, lipid monolayers composed of the zwitterionic DPPC and DOPC were used. To investigate the interaction with bacterial cell membranes, lipid monolayers of anionic DPPG and POPG were used. DPPC and DPPG exhibit a first-order phase transition from the disordered liquid to the ordered condensed state, whereas POPG and DOPC monolayers are in the fluid disordered state at all surface pressures studied. Therefore, the influence of the monolayer phase state on peptide-lipid interactions can be studied. To obtain insight into the peptide structure and their influence on phospholipid membranes, film balance measurements were coupled with surface sensitive Infrared Reflection-Absorption Spectroscopy (IRRAS). The results were compared to CD measurements in bulk.
LL-32 is more surface active and can better intercalate into lipid monolayers than LL-20. Even though LL-32 has no cell-selectivity, our results show how the peptide interacts differently with zwitterionic compared to anionic membrane models. The interaction with DPPC monolayers is based on simple intercalation of the peptides between the lipid molecules. However, the peptides bind in a two-step process to DPPG monolayers, which results in a fluidization of the lipid film. This can be related to a membrane thinning.

**Keywords:** Antimicrobial Peptides, Lipid Monolayers, Fluid Interfaces, FTIR Spectroscopy.

***Corresponding author: Helmuth Möhwald,** Max Planck Institute of Colloids and Interfaces, Science Park Potsdam-Golm, Am Mühlenberg 1, 14476 Potsdam, Germany, e-mail: moehwald@mpikg.mpg.de
**Claudia Dannehl, Gerald Brezesinski:** Max Planck Institute of Colloids and Interfaces, Science Park Potsdam-Golm, Am Mühlenberg 1, 14476 Potsdam, Germany

# 1 Introduction

Antimicrobial peptides (AMPs), also termed host defense peptides, are part of the immune defense system and can be found in every organism [1–3]. Beyond their antibacterial, antifungal and antiviral activities, they are also involved in immunomodulatory activities and inflammatory processes [4, 5] and some are even active against cancer cells [6–8]. AMPs are highly selective and do not attack host cells and thus can be used as lead structures for the development of new drugs complementing standard antibiotic therapies [9, 10]. AMPs kill bacteria within 15 to 90 min [11] and their target is always the membrane. Besides that, antimicrobial peptides can also be involved in biochemical processes like the inactivation of nucleic acids and cytoplasmic proteins [11]. More than thousand AMPs are identified and published in databases [12, 13], but their mode of action is still not completely understood [11, 14, 15].

Several modes of action are discussed for AMPs, including a 'carpet model', or the formation of 'barrel-stave' or 'toroidal pores', where the peptides penetrate the lipid bilayer [6, 12, 16, 17]. For an interaction with the membrane via a 'carpet mechanism', the peptides cover the membrane surface, interact primarily with the lipid head groups, and are oriented parallel to the surface. The formation of a special secondary structure and penetration of the peptides into the hydrophobic core of the bilayer are not mandatory. The membrane is disrupted in a detergent-like way. Polymyxin B is thought to act via that mechanism [18]. The peptides can induce lesions by arranging parallel to the membrane, even without forming pores. But the exact mechanism is still unclear.

One class of amphipathic, cationic, $\alpha$-helical AMPs is the class of cathelicidins. In humans, only one AMP from this class is found, namely LL-37 [19, 20]. LL-37 is released from its precursor hCAP18 by proteases [21] and stored in the intracellular granules of neutrophilic granulocytes [22]. Initially identified solely as an antimicrobial protein, hCAP18/LL-37 is multifunctional with diverse and significant effects on eukaryotic cells [23]. It exhibits hemolytic activity [24, 25] and is cytotoxic against Gram-positive and Gram-negative bacteria [20, 25] as well as tumor cells [26]. LL-37 is also active against viruses [27]. Furthermore, LL-37 can bind and neutralize lipopolysaccharides (LPS) from the cell membrane of Gram-negative bacteria [28, 29]. LL-37 binds as oligomers to zwitterionic membranes [30], but dissociates into monomers when in contact with negatively charged membranes [24].

In a previous study, the surface activity and structures of two fragments (LL-20 and LL-32) of LL-37 at the soft liquid/air interface have been characterized [31]. It was shown that the peptides differ drastically in their surface activity (equilibrium adsorption pressure). As concluded from CD spectra, both peptides are

unstructured in bulk but exhibit different secondary structures when adsorbed to the air/buffer interface [31, 32]. While LL-32 transforms into an $\alpha$-helix lying flat at the buffer surface, with a helix diameter of 17 Å, LL-20 adopts a partly unstructured conformation. The ability of LL-32 to form a perfect $\alpha$-helical structure at the interface is in good agreement with its higher antimicrobial activity.

The experiments with lipid monolayers will examine the influence of lipid charges and packing parameters on the surface activity of the peptide fragments. Moreover, because of the presence of LL-37 in the lung, on the skin, in sweat, and wound fluids [33], the air/buffer interface receives a biological relevance. Two fragments of LL-37, named LL-20 and LL-32, have been used. Both fragments lack the unstructured C-terminal part of the peptide. The antibacterial activity of LL-32 is increased compared to LL-37 [20, 34]. On the contrary, LL-20 exhibits a reduced antibacterial activity [35] compared to LL-37, probably because it lacks the assumed antimicrobial active core LL-37 [18, 29]. LL-32 carries a net charge of +6 (like LL-37), while LL-20 carries a smaller net charge of +4.

Planar lipid films provide a useful model system to study peptide-lipid interactions, if one combines the Langmuir trough technique with surface sensitive methods [36–42].

Zwitterionic phosphatidylcholines (PCs) are often used to model the eukaryotic cell membrane, whereas negatively charged phosphatidylglycerols (PGs) have been used to mimic the cytoplasmic bacterial membrane [43, 44]. Length and degree of saturation of the lipid hydrocarbon tails play a significant role in membrane viscoelastic properties for both mammalian and bacterial cells. The present study is focused on the ability of the peptides to penetrate into different lipid layers, which can give deeper insight into the processes of destroying the bacterial but not the human cell membrane.

The aim of this work is to find decisive differences between the membrane interactions of these fragments.

# 2 Experimental

## 2.1 Materials

Peptides: The two fragments of LL-37, namely LL-20 and LL-32, were synthesized with C-terminal amidation by solid-phase peptide synthesis technique with an automatic peptide synthesizer (model 433 A; Applied Biosystems) on Rink amide resin according to the fastmoc synthesis protocol of the manufacturer, including the removal of the N-terminal Fmoc-group [31]. The peptide was cleaved from the

resin and deprotected and with 90% trifluoroacetic acid (TFA), 5% anisole, 2% thioanisole, 3% dithiothreitol for 3 h at room temperature. After cleavage the suspension was filtered and the soluble peptides were precipitated with ice-cold diethylether followed by centrifugation and extensive washing with ether. Peptides were purified by RP-HPLC using a Jupiter 4$\mu$ Proteo column (Phenomenex). Elution was done by using a gradient of 0%–70% acetonitrile in 0.1% (TFA) to purities above 95%. The purity was determined by analytical reversed-phase HPLC (UV 214 nm) and matrix-assisted laser-desorption-time-of-flight mass spectrometry (MALDI-TOF MS, Bruker). The masses are 3922 Da for LL-32 and 2465 Da for LL-20. The aqueous solutions were prepared using ultrapure water (specific resistance of 18.2 M$\Omega$ cm) produced by a Millipore reverse osmosis unit. Film balance measurements were performed on buffer with 5 mM HEPES (Roth, Germany), pH 7.4, 100 mM NaCl (Merck, Germany, heated to 600 °C before use to remove organic surface active impurities). All experiments were carried out at 20 °C.

Lipids: Zwitterionic 1,2-dipalmitoyl-sn-glycero-3-phosphocholine (DPPC), 1,2-dioleoyl-sn-glycero-3-phosphocholine (DOPC), and anionic 1,2-dipalmitoyl-sn-glycero-3-phospho-(1'-rac-glycerol) (DPPG), 1-palmitoyl-2-oleoyl-sn-glycero-3-phospho-(1'-rac-glycerol) (POPG) were purchased from Avanti Polar Lipids (USA) and stored at −20 °C. For experiments, the lipids were dissolved in chloroform to a concentration of 1 mM and kept at 4 °C.

## 2.2 Langmuir film balance

The adsorption experiments and other studies at the air-water interface were performed in PTFE Langmuir troughs (Riegler & Kirstein, Potsdam, Germany), equipped with barriers for controlling the area per molecule, and a Wilhelmy microbalance with filter paper plate for measuring the surface tension of the monolayer. The temperature of the subphase was kept constant at (20 ± 0.5) °C by a thermostat.

The interaction between peptides and phospholipids was studied by spreading the lipid monolayers on the subphase containing the peptide. The initial surface pressure of the 0.2 μM peptide solution was 0 mN/m. The amount of spread lipids was calculated from their individual $\pi$-A isotherms to give $\pi$ = 0 mN/m. The collection of the surface pressure data was started before spreading.

The maximum insertion pressure (MIP) of LL-32 and LL-20 into lipid monolayers was studied by injection of the corresponding peptide solution underneath a pre-compressed lipid monolayer at a defined surface pressure $\pi_i$. In contrast to the first experiments, the lipid was spread on top of the pure buffer solution, and left for at least 15 min for the solvent evaporation. The formed monolayer was

compressed to a certain surface pressure, and the barriers were stopped. The total area of the surface was kept constant during the adsorption process. Injection of a concentrated peptide stock solution is inexpedient without stirring the subphase because of the formation of a strong concentration gradient. The final peptide concentration after injection into the subphase and careful manual stirring was again 0.2 μM as in the above described experiment. Collection of surface pressure data was started before injection.

### 2.3 Infrared Reflection Absorption Spectroscopy (IRRAS)

IRRA spectra were recorded with the Vertex 70 FT-IR spectrometer (Bruker, Germany) coupled to a Langmuir film balance (Riegler & Kirstein, Germany) with a total area of 182 $cm^2$ and two movable barriers. The surface pressure was measured by using filter paper as a Wilhelmy plate after filling the trough with a 0.2 μM peptide solution. Angles of incidence were varied between 30° and 70°, the polarization of the beam was modulated to perpendicular (s) and parallel (p) polarized light. The reflected IR beam was detected at the same angles with a liquid nitrogen cooled MCT detector. Due to the shuttle technique, a pure subphase spectrum $R_0$ is recorded before the sample spectrum R is measured and the reflectance-absorbance is plotted as $-\lg(R/R_0)$. Therefore, the strong absorption bands from water can be mostly eliminated. Details of the technique can be found in [45–50]. The spectra were atmospheric compensated in OPUS 6.0 and shifted to zero at 1900 $cm^{-1}$. The dichroic ratio was calculated by dividing the intensity of the Amide I band using p-polarized light by that using s-polarized light.

## 3 Results

### 3.1 Interactions of LL-32 and LL-20 with un-compressed monolayers

The corresponding lipid solution is spread on a homogeneous peptide subphase. The amount of lipid used is such that the initial surface pressure is zero (close to the lift-off point of the isotherms determined on the corresponding buffer). The increase in surface pressure with time reflects the peptide adsorption to the interface. Differences in the equilibrium surface pressure give information about the preference of the peptide for the different model membranes [51]. DPPC and

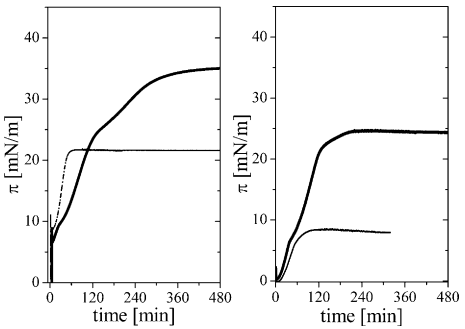


**Figure 1:** Adsorption kinetics of LL-32 (solid) and LL-20 (dotted-dashed) to DPPG (left) DPPC (right) monolayers. 5 mM HEPES, 100 mM NaCl, pH 7.4, 20 °C, 0.2 μM peptide in solution.

DPPG (both lipids exhibit a first-order LE/LC transition on the buffer used) have been used to mimic mammalian or bacteria cell membranes, respectively.

Spreading of the DPPG solution on the peptide-containing subphase leads to a strong increase in the surface pressure (Figure 1 left).

A small plateau in the $\pi = f(t)$ adsorption kinetics can be seen for both peptides connected with the LE/LC phase transition of DPPG around 10 mN/m. A second plateau at 25 mN/m must be connected with reorientation processes within the mixed surface layer. The equilibrium pressure for both peptides is increased in the presence of DPPG (35 mN/m compared to 25 mN/m for LL-32 alone; 22 mN/m compared to 6 mN/m for LL-20 alone). The equilibrium surface pressure is reached much faster for the less active LL-20, indicating additional interactions of LL-32 with DPPG.

The peptide adsorption to DPPC (Figure 1 right) leads to a surface pressure increase of 8.5 mN/m in the presence of LL-20, and to 25 mN/m in the presence of LL-32. These values are comparable with the peptide equilibrium pressures at the bare air/buffer interface, indicating the absence of specific interactions of the peptides with DPPC. The adsorption kinetics of LL-32 shows again a small plateau connected with the first-order LE/LC phase transition in the DPPC monolayer. In the case of LL-20, the peptide adsorption leads only to a surface pressure close to the transition pressure so that the plateau cannot be observed.

IRRAS experiments have been used to identify the phase of the lipid monolayers. Both peptides lead to a fluidization of the DPPG monolayer. After reaching the adsorption equilibrium, the position and the dichroic ratio of the asymmetric $CH_2$ vibrational bands agree well with those of a DPPG monolayer in a liquid-expanded phase (Figure 2). This is surprising, since the equilibrium pressure is much higher than the phase transition pressure of a DPPG monolayer on the bare buffer (~10 mN/m).

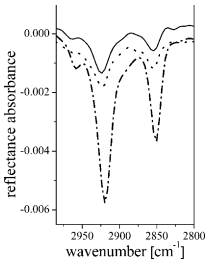


**Figure 2:** $CH_2$ stretching vibrations of mixed DPPG/LL-32 films at $\pi_{eq} = 35$ mN/m (solid line, shifted upwards for clarity) and LL-20 at $\pi_{eq} = 22$ mN/m (dotted) and $\pi = 30$ mN/m (dotted-dashed). 5 mM HEPES, 100 mM NaCl, pH 7.4, 20 °C, 0.2 μM peptide in solution.

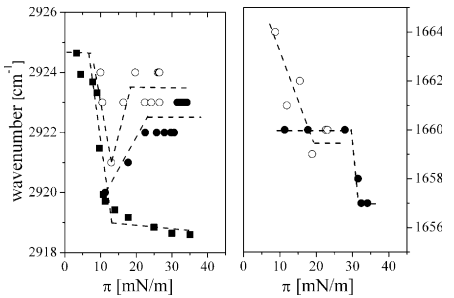


**Figure 3:** Maxima of the asymmetric $CH_2$ vibrational band (left) and maxima of the amide I band (right) as a function of the surface pressure $\pi$ for DPPG (■) as well as DPPG/LL-32 (●) and DPPG/LL-20 (○). 5 mM HEPES, 100 mM NaCl, pH 7.4, 20 °C, 0.2 μM peptide in solution. The lines are only to guide the eye.

During the adsorption process (Figure 1), the adsorption/penetration of LL-32 induces first the LE/LC transition of DPPG (small plateau in the $\pi = f(t)$ curve and the shift of $\nu_{as}(CH_2)$ to lower wavenumbers (2920 cm$^{-1}$ at 10 mN/m)) which is followed by a fluidization of the DPPG layer with $\nu_{as}(CH_2)$ at 2923 cm$^{-1}$ (expanded state) for surface pressures >20 mN/m (Figure 3 left). LL-20, which adsorbs much faster, shifts first the methylene vibration to 2921 cm$^{-1}$ (condensed state) which then increases again to 2923 cm$^{-1}$ (expanded state) for surface pressures >15 mN/m. This indicates clearly that the peptide adsorption leads first to an alkyl chain ordering due to increased packing densities and then to a fluidization due to specific peptide-lipid interactions. Therefore, the second 'plateau' in the adsorption kinetics above 25 mN/m might also be connected with the reentrant transition into the LE phase.

The DPPG/LL-20 film ($\pi_{eq} \sim 22$ mN/m) could be further compressed to 30 mN/m. The asymmetric $CH_2$ band position shifts back to 2920 cm$^{-1}$. This

shows that a squeezing-out of the peptide occurs above $\pi_{eq}$ allowing the re-condensation of the DPPG layer.

During the adsorption process, a shift in the amide I band position to lower frequencies (Figure 3 right) has been observed. A red-shift in the amide I band position can be attributed to the formation of hydrogen bonds [44, 52, 53] or a change in the helix flexibility [54]. Also, a change in the backbone hydration influences slightly the band position. This can be due to an aggregation of the peptide [55–57] or a deeper incorporation into the hydrophobic environment. Both events are connected with the partial dehydration of the C=O groups. As shown in [31], LL-20 adopts a less distinct $\alpha$-helix with more contact to water. The stronger shift for LL-32/DPPG mixtures could be therefore explained by a deeper insertion of LL-32 compared to LL-20 or simply by the formation of a more perfect $\alpha$-helix in contact with DPPG. In equilibrium, the amide I band can be fitted with two Lorentzian curves with maxima at 1657.8 $cm^{-1}$ and 1679 $cm^{-1}$ for LL-32 and 1658.1 $cm^{-1}$ and 1668.2 $cm^{-1}$ for LL-20. The high energy band can be attributed to the vibration of non-hydrogen bonded C=O groups [58].

To compare the orientation of the peptides, the dichroic ratio (intensity of the p-polarized light divided by the intensity of the s-polarized light) of the amide I band has been analyzed [50, 59]. It is independent of the concentration or length of the peptides and allows comparisons regarding the orientation in both, in-plane and out-of-plane directions. The dichroic ratio of the amide I band is comparable for both peptides, indicating that both peptides adopt the same orientation when interacting with DPPG. But the values are slightly below the values expected for a complete $\alpha$-helix lying flat at the air/water interface [31].

The interaction of the peptides with zwitterionic DPPC is clearly different from that with the anionic DPPG (compare the adsorption kinetics). LL-32 adsorbs at the interface and compresses the DPPC layer into the condensed state. The LE/LC transition can be already seen in the adsorption kinetics. The methylene stretching vibrations (Figure 4 left) shift to wavenumbers ($\nu_{as} \sim 2919\ cm^{-1}$ and $\nu_s \sim 2850\ cm^{-1}$) indicative for the all-trans conformation of the alkyl chains. The band intensity increases due to increased packing density and to the change in the orientation of the transition dipole moment by undergoing the fluid-condensed transition [53]. The dichroic ratio of DPPC/LL-32 agrees well with the value of a pure DPPC film at the same surface pressure indicating a similar monolayer structure. The adsorption of LL-20 leads to a lateral pressure of only 7.5 mN/m, at which DPPC is still in the LE phase indicated by the high wavenumbers of the $CH_2$ stretching bands ($\nu_{as} \sim 2923\ cm^{-1}$ and $\nu_s \sim 2854\ cm^{-1}$). The presence of both peptides at the interface can be detected by the appearance of amide bands (Figure 4 right).

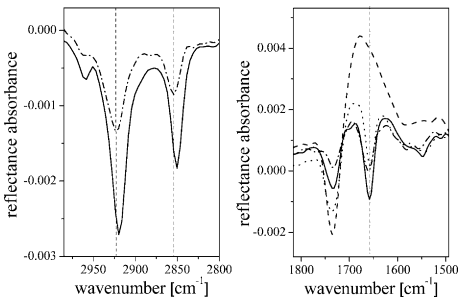


**Figure 4:** $CH_2$ band region (left) and amide I band region (right) of DPPC/peptide mixtures. DPPC/LL-32 at $\pi_{eq}$ = 25 mN/m (solid) and $\pi$ = 30 mN/m (dotted), DPPC/LL-20 at $\pi_{eq}$ = 7.5 mN/m (dotted-dashed) and $\pi$ = 30 mN/m (dashed). 5 mM HEPES, 100 mM NaCl, pH 7.4, 20 °C, 0.2 μM peptide in solution.

Compression of the mixed peptide/DPPC films to 30 mN/m leads to a shift to lower wavenumbers of the $CH_2$ stretching vibrations as observed for the pure condensed DPPC film at the bare air/buffer interface. The less effective LL-20 is completely squeezed-out from the DPPC film (absence of amide bands, see Figure 4 right). This is not the case for LL-32. The presence of amide bands in the spectra indicates that LL-32 is still located at the interface and influences the lipid monolayer structure. However, the amide band intensity is decreased and the ester band of DPPC is increased indicating that at least a part of LL-32 is squeezed-out and replaced by DPPC.

## 3.2 Interactions of LL-32 and LL-20 with pre-compressed monolayers

Maximum Insertion Pressure (MIP) measurements using lipid monolayers compressed to a defined target pressure $\pi_i$ are an easy method to assess if a peptide is able to penetrate into the membrane. The peptide is injected underneath the pre-compressed monolayer keeping the surface area constant. An interaction of the peptide with the lipids leads to a change in the surface pressure $\pi$. The change of the surface pressure $\Delta\pi = \pi - \pi_i$ is plotted as a function of the initial pressure $\pi_i$. A linear fitting and extrapolating to $\Delta\pi = 0$ gives the MIP up to which the penetration of the peptide into the lipid monolayer is energetically favorable [60, 61]. If this value is higher or in the range of the lateral pressure in a bilayer, found to be between 30 and 35 mN/m [62, 63], then the peptide can insert into a biological membrane. The slope of the linear fit provides further information on the way the peptide interacts with the lipid layer. Two scenarios are possible [64, 65]. Either

$\Delta\pi$ is independent of $\pi_i$ indicating that the peptide penetrates into the layer at each initial surface pressure $\pi_i$. In this case, the equilibrium surface pressure $\pi_{eq}$ of the mixed lipid/peptide system increases with increasing $\pi_i$. A stationary $\pi_{eq}$ leads to a reduced increase in $\Delta\pi$ with increasing $\pi_i$, meaning that it is more difficult for the peptide to penetrate into a compressed monolayer.

The change in surface pressure after the injection of LL-32 and LL-20 has been monitored, and the corresponding $\Delta\pi$ versus $\pi_i$ curves for DPPG, DPPC, POPG and DOPC monolayers are shown in Figures 5 and 6. A slope different from −1 indicates that the equilibrium pressure is not stationary but depends on the starting pressure $\pi_i$.

In the experiments with LL-32 and the fluid monolayers of DOPC and POPG, irregularities can be seen in the adsorption kinetics. Film instabilities might be the

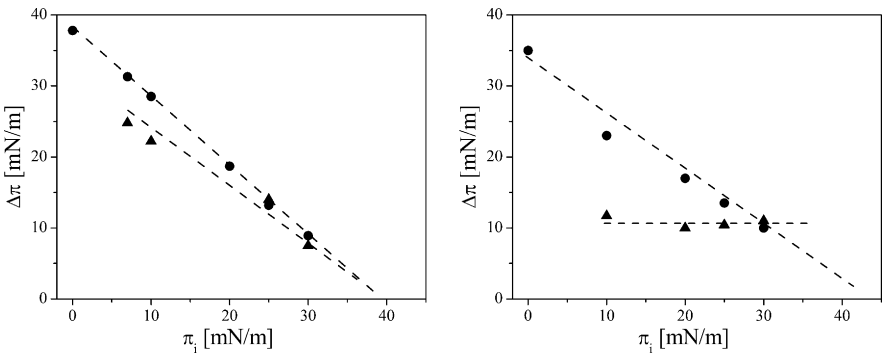


**Figure 5:** MIP experiments with LL-20 (▲) and LL-32 (●) into negatively charged POPG (left) and DPPG (right) monolayers. Extrapolating the linear fit of $\Delta\pi = \pi - \pi_i$ versus $\pi_i$ to $\Delta\pi = 0$ gives the MIP. 5 mM HEPES, 100 mM NaCl, pH 7.4, 20 °C, 0.2 μM peptide in solution.

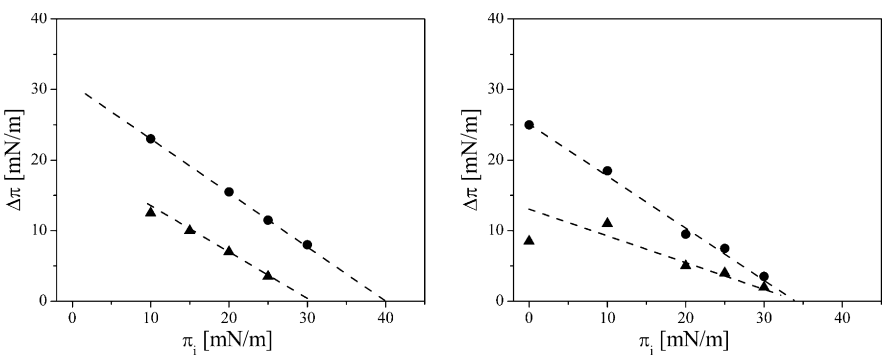


**Figure 6:** MIP experiments with LL-20 (▲) and LL-32 (●) into zwitterionic DOPC (left) and DPPC (right) monolayers. Extrapolating the linear fit of $\Delta\pi = \pi - \pi_i$ versus $\pi_i$ to $\Delta\pi = 0$ gives the MIP. 5 mM HEPES, 100 mM NaCl, pH 7.4, 20 °C, 0.2 μM peptide in solution.

**Table 1:** Maximum Insertion Pressure (MIP), and slope of the linear fit.

| peptide | phospholipid | MIP [mN/m] | slope |
|---|---|---|---|
| LL-32 | DPPG | 45 ± 5 | −1 |
| | DPPC | 35 ± 2 | −0.7 |
| | POPG | 40 ± 2 | −1 |
| | DOPC | 42 ± 2 | −0.7 |
| LL-20 | DPPG | undefined | 0 |
| | DPPC | 32 ± 3 | −0.5 |
| | POPG | 38 ± 3 | −0.9 |
| | DOPC | 30 ± 2 | −0.7 |

reason [66, 67]. LL-32 is strongly attracted by the fluid lipid monolayers and accumulates quickly at the interface. This leads to local destabilization of the lipid monolayer which results in the drop of the surface pressure. Due to further adsorption of peptides, the surface pressure increases again leading to additional defects until the adsorption equilibrium of the peptide is reached.

The MIP and slope values are listed in Table 1. LL-32 has a high affinity for negatively charged lipid monolayers. The injection of LL-32 under pre-compressed POPG and DPPG monolayers leads to a strong increase in the surface pressure. The equilibrium pressure $\pi_{eq}$ is a stationary surface pressure and the monolayer phase has no strong influence on $\Delta\pi$ and the MIP [65]. The MIP of LL-32 is (45 ± 3) mN/m for DPPG and (40 ± 2) mN/m for POPG.

The injection of LL-20 underneath a DPPG monolayer leads to a constant increase of $\Delta\pi$ = 10 mN/m for all $\pi_i$, which yields an infinite MIP reflecting only electrostatic attraction and no hydrophobic interactions, because of the independence from the lipid packing density (phase state). The peptide is attracted to the charged head groups but exhibits no further interaction with the lipids. The peptide could be inactivated by hindering electrostatic interactions. The effect of LL-20 on POPG monolayers is comparable with that of LL-32. The MIP is 38 mN/m.

The MIP of LL-20 into DPPC monolayers is (32 ± 3) mN/m. Together with the small slope of −0.5, it is obvious that LL-20 has only a low affinity for DPPC. The same holds for DOPC monolayers. Obviously, LL-20 cannot penetrate into zwitterionic lipid monolayers at physiologically relevant surface pressures (30–35 mN/m), independent of the lipid phase. LL-32 has a slightly higher MIP of (35 2)mN/m into DPPC with a slope of −0.7, indicating an interaction with the zwitterionic DPPC at low lateral pressures. The MIP of LL-32 into DOPC monolayers is much higher and even comparable with that of POPG and is in agreement with the non-pronounced cell selectivity of this peptide [24].

IRRAS measurements at the air/water interface have been performed additionally to the MIP experiments using the more active peptide LL-32. They are extremely useful to examine if the interaction of the peptides with the lipids leads to changes in the peptide secondary structure and the phase of the lipids. The $CH_2$ stretching vibrational band positions reflect the order in the hydrophobic chain region. The amide bands are connected with the secondary structure of the peptide. The OH-band intensity is related to the film thickness [52] and is therefore influenced by the lipid tilt angle in condensed phases and the formation of adsorption layers.

The spectra of the condensed DPPG film (Figure 7) show a small increase in the $\nu$(OH) band intensity on increasing the lateral pressure. This increase in the lipid monolayer thickness is directly connected with the reduction of the tilt angle determined by GIXD experiments [68].

Above 8 mN/m, DPPG is in a condensed state with an all-trans conformation of the alkyl chains. The phase of the lipids can be deduced from the band position of the symmetric and asymmetric $CH_2$ stretching vibrations. Values of 2919 $cm^{-1}$ for the $\nu_{as}(CH_2)$ and 2849 $cm^{-1}$ for the $\nu_s(CH_2)$ have been observed both before and after peptide injection showing that the state of the lipids is not affected by the peptide. This is in contrast to the experiments with un-compressed DPPG monolayers. There peptide injection leads to a drastic increase of the OH-band which could be caused by an increase of the lipid packing density connected with a decrease of the tilt angle and the formation of an additional peptide adsorption layer underneath the lipid head groups. At the same time, amide bands (amide A ~3300 $cm^{-1}$, amide I ~1658 $cm^{-1}$) appear. The amide I band position at

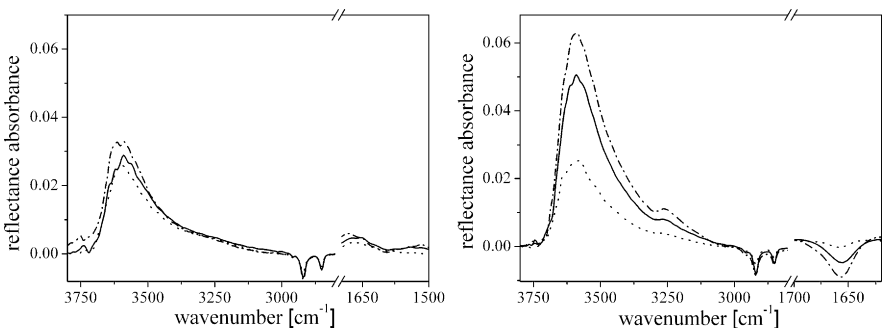


**Figure 7:** IRRA spectra of DPPG (left) and DPPG/LL-32 mixed films (right). The peptide was injected under a pre-compressed monolayer with $\pi_i$ of 10 mN/m (dotted), 20 mN/m (solid) or 30 mN/m (dotted-dashed). The spectra were measured after reaching the equilibrium pressure: p-polarized light, 40° incidence angle, 5 mM HEPES, 100 mM NaCl, pH 7.4, 20 °C, 0.2 μM peptide in solution.

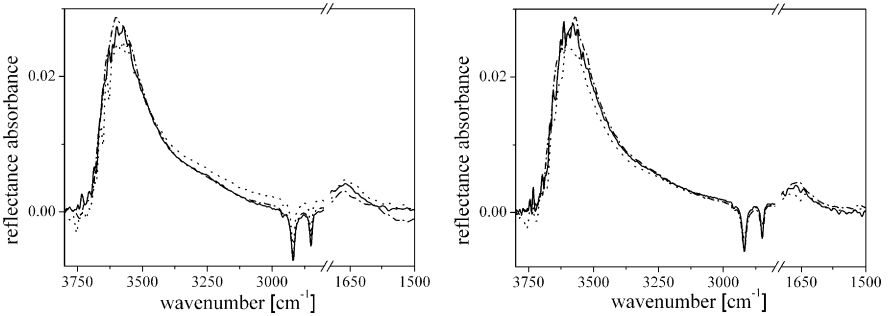


**Figure 8:** IRRA spectra of DPPC (left) and DPPC/LL-32 mixed films (right). The peptide was injected under a pre-compressed monolayer with $\pi_i$ of 10 mN/m (dotted), 20 mN/m (solid), or 30 mN/m (dotted-dashed). The spectra were measured after reaching the equilibrium pressure: p-polarized light, 40° incidence angle, 5 mM HEPES, 100 mM NaCl, pH 7.4, 20 °C, 0.2 μM peptide in solution.

~1658 $cm^{-1}$ denotes the presence of the peptide with most probably an $\alpha$-helical structure.

In the case of POPG, the alkyl chains are in a disordered fluid state at 20 °C leading to $\nu_s(CH_2) = 2855\ cm^{-1}$ and $\nu_{as}(CH_2) = 2923\ cm^{-1}$. The intensity of these bands is quite low because of the low lipid density in the LE phase and the not well oriented transition dipole moments [69]. The presence of amide bands illustrates the presence of the peptide in or close to the lipid film. The intensity of the $\nu$(OH) of POPG is almost unchanged after peptide injection, indicating a complete incorporation of the peptide into the lipid film and no formation of an additional adsorption layer underneath the lipid head groups as observed for DPPG.

In DPPC/L-32 mixed films (Figure 8), no amide bands were detected for $\pi_i >$ 10 mN/m. For $\pi_i = 10$ mN/m only a small dip in the spectrum at 1658 $cm^{-1}$ can be seen. Apart from that, the increase in the surface pressure after the peptide injection ($\pi_{eq} > \pi_i$) denotes a certain interaction of the peptide with the lipid interface. The question arises why this peptide cannot be seen in IRRAS experiments. An explanation for this could be that the peptide binds preferentially to the air/water interface without specific interactions with the DPPC molecules. This assumption is supported by the fact that the equilibrium pressure of the peptide at the bare air/buffer interface is very similar to that at the air/lipid interface. The mixed system is then phase-separated and peptide patches could be located outside the IR spot.

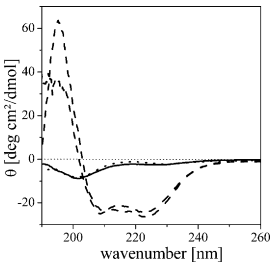


**Figure 9:** CD spectra of LL-32 and LL-20 in water at 20 °C in the presence of POPC vesicles (solid line for LL-32 and dotted line for LL-20) and in the presence of POPG vesicles (dashed lines, LL-20 has the higher intensity around 195 nm). Peptide:lipid = 1 : 16.

### 3.3 Comparison to measurements in bulk

CD experiments have been performed with the peptides and lipid vesicles (Figure 9). Due to the high absorbance of NaCl and HEPES in CD spectroscopy, the experiments were performed in ultrapure water [70]. Both peptides are unstructured in water. The helical content was calculated to be <1% for both peptides, also for a NaCl concentration of 100 mM. The addition of POPC vesicles to the peptide solution has only little effect on the peptide conformation. The CD spectra correspond still to an unstructured peptide [70, 71], although the intensity at 230 nm is slightly increased. However, the addition of POPG vesicles leads to a drastic change in the peptide conformation of both LL-32 and LL-20. A positive band at 193 nm and two negative bands at 207 and 222 nm emerge. These bands are indicators for an $\alpha$-helix [70–72]. A formation of transmembrane pores in equilibrium can be excluded, since transmembrane pores lead to a red-shift of the positive band in the range of 195–200 nm and a higher intensity of the band at 222 nm compared to that at 208 nm [72, 73].

## 4 Discussion

The peptides used are fragments of the human antimicrobial LL-37 and show contrary behavior in biological experiments. While LL-32 is more active compared to the mother peptide, LL-20 is active only at very high concentrations [74]. Lipid monolayers composed of DPPG, POPG, DPPC and DOPC were used to clarify how the lipid charge and the lipid phase influence the lipid/peptide interactions. Surface sensitive IRRAS was coupled to Langmuir film balance measurements to ob-

tain details on a molecular level. The results can be compared with CD experiments with vesicles composed of POPC and POPG, respectively.

Both peptides are surface active. This surface activity is enhanced by the presence of lipids. The equilibrium surface pressure for LL-32 at a lipid covered surface is quite high (35 mN/m with DPPG and 25 mN/m with DPPC). LL-20 is less surface active and exhibits smaller equilibrium surface pressures in the presence of lipids (22 mN/m with DPPG and 8.5 mN/m with DPPC).

Maximum Insertion Pressure (MIP) measurements revealed the critical surface pressure, up to which the peptides penetrate into lipid monolayers. For a successful interaction with a cell membrane, the MIP should be higher than 30–35 mN/m (internal lateral pressure in a membrane [62, 63]). The low MIPs of LL-20 into DOPC and DPPC monolayers indicate that the peptide will not spontaneously insert into zwitterionic regions of cell membranes. The interaction of LL-20 with negatively charged lipid monolayers is dependent on the lipid phase. Injection of LL-20 under pre-compressed DPPG monolayers led to a constant increase in the surface pressure, independent of the initial surface pressure $\pi_i$. The higher charge density of a condensed DPPG layer compared to the lower charge density of a fluid POPG layer leads to strong electrostatic attraction, but the higher molecular density prevents the penetration of LL-20 into the tightly packed hydrophobic layer region. LL-32 shows a strong affinity for both zwitterionic and negatively charged lipid monolayers and an interaction at physiologically relevant surface pressures of 30–35 mN/m. LL-32 completely penetrates the fluid POPG monolayers for $\pi <$ MIP, but forms an additional adsorption layer underneath the DPPG monolayers.

The differences in the surface activity and MIPs for different lipids are indicative for a different way of action of the peptides [51] and the selectivity of the peptide towards different membrane compositions. Both peptides have no influence on DPPC monolayers. The $CH_2$ band positions of the mixed DPPC/peptide films are the same as for DPPC at the bare air/buffer interface. The peptides most probably adsorb in clusters and lead to a phase-separated system. Compression of the mixed films leads to a complete squeezing-out of LL-20, but not of LL-32 (the amide I band is still present).

For DPPG monolayers, the $CH_2$ band position in the IRRA spectra is indicative for an expanded lipid phase proving the fluidization of the lipid film. During the adsorption process, the peptide occupies space at the surface, compresses the DPPG molecules and triggers the LE/LC phase transition. The highly charged condensed lipid domains serve as a target for further peptide-lipid interaction. While the peptide completely incorporates into pre-compressed POPG films, the peptide injection under DPPG monolayers leads to additional binding underneath the head groups. The peptide is electrostatically bound to the head groups, but pos-

sibly with an irregular conformation. Both peptides adopt $\alpha$-helical conformation with a comparable orientation, as concluded from the amide I band position and the corresponding dichroic ratio.

Both peptides are unstructured in solution, but adopt helical conformation when bound to POPG vesicles. POPC vesicles have no effect on the secondary structure of LL-20 and LL-32 in water, indicated by almost unchanged CD spectra. To estimate, if the unstructured peptides can bind to POPC vesicles, some simple calculations can be performed with the help of Mpex [75] by using the White-Wimley scale [76]. This allows evaluating if the adsorption of the unstructured peptides to a hydrophilic-hydrophobic interface is energetically favorable. The Gibbs energy $\Delta G_{wif}$ for the transition of the unstructured peptides from water to a POPC interface amounts to 6.86 kcal/mol for LL-20 and 9.28 kcal/mol for LL-32, indicating that binding of the unstructured peptide to POPC is energetically unfavorable. $\Delta G$ can be reduced by the formation of hydrogen bonds with the formation of $\alpha$-helices, which reduces $\Delta G$ to $-0.4$ kcal/mol per residue [77]. Therefore, a helical content of ≥73% for LL-32 and ≥86% for LL-20 would be needed for a favorable interaction.

# 5 Conclusions

LL-32 and LL-20 are two fragments of the human antimicrobial LL-37. They show a contrary behavior in biological experiments. To obtain information about the secondary structure of the peptides in bulk and confined to the air/liquid interface, CD and IRRAS experiments have been performed, respectively Lipid monolayers (2D system) and lipid vesicles (3D system) were used as simple models for the outer leaflet of a cell membrane.

LL-32 is more surface active and can better intercalate into lipid monolayers compared to LL-20. Even though LL-32 has no cell-selectivity, our results show that the peptide interacts differently with zwitterionic compared to anionic model membranes. The interaction with DPPC monolayers is based on the simple intercalation of the peptides between the lipid molecules, which leads to a phase transition of the lipids to a condensed phase. The interaction of LL-32 with zwitterionic lipids is in line with the observed haemolytic properties [74]. The observation that LL-32 is able to fluidize negatively charged DPPG monolayers is extremely important. However, this is only observed for un-compressed DPPG layers. The penetrated peptides compress the film and induce the LE/LC phase transition allowing more peptide to adsorb at the interface. The larger amount of peptide leads to the

re-appearance of the LE phase. At the moment, the question why LL-32 does not fluidize pre-compressed condensed DPPG monolayers remains unanswered.

**Acknowledgement:** We thank Prof. Thomas Gutsmann (Research Center Borstel, Leibniz-Center for Medicine and Biosciences, Priority Area Infections, Biophysics) for providing the peptide fragments and helpful discussions.

## References

1. L. S. Tavares, O. M. de Santos, L. F. Viccini, J. S. Moreira, R. N. Miller, and O. L. Franco, Peptides **29** (2008) 1842.
2. A. Giuliani, G. Pirri, A. Bozzi, A. di Giulio, M. Aschi, and A. C. Rinaldi, Cell. Mol. Life Sci. **65** (2008) 2450.
3. M. Zasloff, Nature **415** (2002) 389.
4. Y. P. Lai and R. L. Gallo, Trends Immunol. **30** (2009) 131.
5. J. Schauber and R. L. Gallo, J. Allergy Clin. Immun. **122** (2008) 261.
6. S. B. Coffelt, R. S. Waterman, L. Florez, K. H. Z. Bentrup, K. J. Zwezdaryk, S. L. Tomchuck, H. L. LaMarca, E. S. Danka, C. A. Morris, and A. B. Scandurro, Int. J. Cancer **122** (2008) 1030.
7. J. D. Heilborn, M. F. Nilsson, C. I. C. Jimenez, B. Sandstedt, N. Borregaard, E. Tham, O. E. Sørensen, G. Weber, and M. Ståhle, Int. J. Cancer **114** (2005) 713.
8. J. von Haussen, R. Koczulla, R. Shaykhiev, C. Herr, O. Pinkenburg, D. Reimer, R. Wiewrodt, S. Biesterfeld, A. Aigner, F. Czubayko, and R. Bals, Lung Cancer **59** (2008) 12.
9. D. W. Hoskin and A. Ramamoorthy, BBA-Biomembranes **1778** (2008) 357.
10. H. Schröder-Borm, R. Bakalova, and J. Andrä, FEBS Lett. **579** (2005) 6128.
11. K. A. Brogden, Nat. Rev. Microbiol. **3** (2005) 238.
12. A. Tossi, L. Sandri, and A. Giangaspero, Biopolymers **55** (2000) 4.
13. G. S. Wang, X. Li, and Z. Wang, Nucleic Acids Res. **37** (2009) D933.
14. Y. Shai, Biochim. Biophys. Acta **1462** (1999) 55.
15. K. Hristova, C. E. Dempsey, and S. H. White, Biophys. J. **80** (2001) 801.
16. Y. Huang, J. Huang, and Y. Chen, Protein Cell **1** (2010) 143.
17. N. Papo and Y. Shai, Peptides **24** (2003) 1693.
18. A. Wiese, M. Münstermann, T. Gutsmann, B. Lindner, K. Kawahara, U. Zähringer, and U. Seydel, J. Membrane Biol. **162** (1998) 127.
19. M. Zanetti, Curr. Issues Mol. Biol. **7** (2005) 179.
20. J. W. Larrick, M. Hirata, J. Zhong, and S. C. Wright, Immunotechnology **1** (1995) 65.
21. G. S. Wang, J. Biol. Chem. **283** (2008) 32637.
22. J. B. Cowland, A. H. Johnsen, and N. Borregaard, FEBS Lett. **368** (1995) 173.
23. G. Weber, C. I. Chamorro, F. Granath, A. Liljegren, S. Zreika, Z. Saidak, B. Sandstedt, S. Rotstein, R. Mentaverri, F. Sanchez, A. Pivarcsi, and M. Stahle, Breast Cancer Res. **11** (2009) R6.
24. Z. Oren, J. C. Lerman, G. H. Gudmundsson, B. Agerberth, and Y. Shai, Biochem. J. **341** (1999) 501.

25. S. M. Travis, N. N. Anderson, W. R. Forsyth, C. Espiritu, B. D. Conway, E. P. Greenberg, P. B. McCray, R. I. Lehrer, M. J. Welsh, and B. F. Tack, Infect. Immun. **68** (2000) 2748.
26. K. Okumura, A. Itoh, E. Isogai, K. Hirose, Y. Hosokawa, Y. Abiko, T. Shibata, M. Hirata, and H. Isogai, Cancer Lett. **212** (2004) 185.
27. S. Tripathi, T. Tecle, A. Verma, E. Crouch, M. White, and K. L. Hartshorn, J. Gen. Virol. **94** (2012) 40.
28. J. W. Larrick, M. Hirata, R. F. Balint, J. Lee, J. Zhong, and S. C. Wright, Infect. Immun. **63** (1995) 1291.
29. Y. H. Nan, J. K. Bang, B. Jacob, I. S. Park, and S. Y. Shin, Peptides **35** (2012) 239.
30. A. Ramamoorthy, D. K. Lee, J. S. Santos, and K. A. Henzler-Wildman, J. Am. Chem. Soc. **130** (2008) 11023.
31. C. Dannehl, T. Gutsmann, and G. Brezesinski, Colloid. Surface. B **109** (2013) 129.
32. C. Dannehl, O. Travkova, and G. Brezesinski, Chem. Lett. **41** (2012) 1178.
33. U. H. N. Durr, U. S. Sudheendra, and A. Ramamoorthy, BBA-Biomembranes **1758** (2006) 1408.
34. T. Gutsmann, S. O. Hagge, J. W. Larrick, U. Seydel, and A. Wiese, Biophys. J. **80** (2001) 2935.
35. M. H. Braff, M. A. Hawkins, A. Di Nardo, B. Lopez-Garcia, M. D. Howell, C. Wong, K. Lin, J. E. Streib, R. Dorschner, D. Y. M. Leung, and R. L. Gallo, J. Immunol. **174** (2005) 4271.
36. H. Brockman, Curr. Opin. Struc. Biol. **9** (1999) 438.
37. R. Maget-Dana, BBA-Biomembranes **1462** (1999) 109.
38. H. Möhwald, Annu. Rev. Phys. Chem. **41** (1990) 441.
39. G. Brezesinski and H. Möhwald, Adv. Colloid Interfac. **100-102** (2003) 563.
40. G. Thakur, M. Micic, and R. M. Leblanc, Colloid. Surface. B **74** (2009) 436.
41. C. Stefaniu, G. Brezesinski, and H. Möhwald, Adv. Colloid Interfac. **208** (2014) 197.
42. C. Stefaniu and G. Brezesinski, Adv. Colloid Interfac. **207** (2014) 265.
43. K. Lohner, *Development of Novel Antimicrobial Agents: Emerging Strategies*, Horizon Scientific Press, Norfolk (2001).
44. O. G. Travkova, J. Andrä, H. Möhwald, and G. Brezesinski, Langmuir **29** (2013) 12203.
45. C. R. Flach, J. W. Brauner, J. W. Taylor, R. C. Baldwin, and R. Mendelsohn, Biophys. J. **67** (1994) 402.
46. R. Mendelsohn, J. W. Brauner, and A. Gericke, Annu. Rev. Phys. Chem. **46** (1995) 305.
47. C. R. Flach, A. Gericke, and R. Mendelsohn, J. Phys. Chem. B **101** (1997) 58.
48. A. H. Muenter, J. Hentschel, H. G. Börner, and G. Brezesinski, Langmuir **24** (2008) 3306.
49. T. D. Andreeva, J. G. Petrov, G. Brezesinski, and H. Möhwald, Langmuir **24** (2008) 8001.
50. R. Mendelsohn, G. Mao, and C. R. Flach, BBA-Biomembranes **1798** (2010) 788.
51. P. Bougis, H. Rochat, G. Pieroni, and R. Verger, Biochemistry **20** (1981) 4915.
52. O. G. Travkova, J. Andrä, H. Möhwald, and G. Brezesinski, ChemPhysChem **11** (2010) 3262.
53. S. T. R. Walsh, R. P. Cheng, W. W. Wright, D. O. V. Alonso, V. Daggett, J. M. Vanderkooi, and W. F. DeGrado, Protein Sci. **12** (2003) 520.
54. Y. P. Zhang, R. N. A. H. Lewis, R. S. Hodges, and R. N. McElhaney, Biochemistry **31** (1992) 11579.
55. S. Mukherjee, P. Chowdhury, and F. Gai, J. Phys. Chem. B **111** (2007) 4596.
56. M. Albrecht, C. A. Rice, and M. A. Suhm, J. Phys. Chem. A **112** (2008) 7530.
57. R. Ludwig, O. Reis, R. Winter, F. Weinhold, and T. C. Farrar, J. Phys. Chem. B **102** (1998) 9312.
58. L. K. Tamm and S. A. Tatulian, Q. Rev. Biophys. **30** (1997) 365.

59. M. Hoernke, J. A. Falenski, C. Schwieger, B. Koksch, and G. Brezesinski, Langmuir **27** (2011) 14218.
60. P. Calvez, S. Bussieres, E. Demers, and C. Salesse, Biochimie **91** (2009) 718.
61. O. G. Travkova and G. Brezesinski, Chem. Phys. Lipids **167** (2013) 43.
62. D. Marsh, BBA-Rev. Biomembranes **1286** (1996) 183.
63. A. Blume, Biochim. Biophys. Acta **557** (1979) 32.
64. P. Calvez, E. Demers, E. Boisselier, and C. Salesse, Langmuir **27** (2011) 1373.
65. E. Boisselier, P. Calvez, E. Demers, L. Cantin, and C. Salesse, Langmuir **28** (2012) 9680.
66. F. Neville, M. Cahuzac, O. Konovalov, Y. Ishitsuka, K. Y. C. Lee, I. Kuzmenko, G. M. Kale, and D. Gidalevitz, Biophys. J. **90** (2006) 1275.
67. D. Gidalevitz, Y. Ishitsuka, A. S. Muresan, O. Konovalov, A. J. Waring, R. I. Lehrer, and K. Y. Lee, P. Natl. Acad. Sci. USA **100** (2003) 6302.
68. E. Maltseva, V. L. Shapovalov, H. Möhwald, and G. Brezesinski, J. Phys. Chem. B **110** (2006) 919.
69. A. Meister, A. Kerth, and A. Blume, J. Phys. Chem. B **109** (2005) 6239.
70. S. M. Kelly, T. J. Jess, and N. C. Price, BBA-Proteins Proteom. **1751** (2005) 119.
71. C. Olak, A. Muenter, J. Andrä, and G. Brezesinski, J. Pept. Sci. **14** (2008) 510.
72. F. Bringezu, M. Majerowicz, E. Maltseva, S. Y. Wen, G. Brezesinski, and A. J. Waring, ChemBioChem **8** (2007) 1038.
73. K. Park, A. Perczel, and G. D. Fasman, Protein Sci. **1** (1992) 1032.
74. M. U. Hammer, PhD thesis, Christian-Albrechts-Universität Kiel (2007).
75. C. Snider, S. Jayasinghe, K. Hristova, and S. H. White, Protein Sci. **18** (2009) 2624.
76. S. H. White and W. C. Wimley, BBA-Rev. Biomembranes **1376** (1998) 339.
77. A. S. Ladokhin and S. H. White, J. Mol. Biol. **285** (1999) 1363.